Rapid Communications in Mass Spectrometry

WILEY

Rapid Communications in Mass Spectrometry

RESEARCH ARTICLE OPEN ACCESS

A High-Precision Analytical Technique for Dissolved N_2 Isotopes in Aquatic Systems: Biogeochemical Applications and Determination of Solubility Equilibrium Isotope Effects

Katelyn McPaul[1,2] | Scott D. Wankel[2] | Alan M. Seltzer[2]

[1]MIT-WHOI Joint Program in Oceanography/Applied Ocean Science and Engineering, Cambridge and Woods Hole, Massachusetts, USA | [2]Marine Chemistry and Geochemistry Department, Woods Hole Oceanographic Institution, Woods Hole, Massachusetts, USA

Correspondence: Katelyn McPaul (katelyn.mcpaul@whoi.edu)

Received: 3 March 2025 | **Revised:** 30 May 2025 | **Accepted:** 6 June 2025

Funding: This work was supported by National Science Foundation (OCE-2318938) and Andrew W. Mellon Foundation.

Keywords: biogeochemistry | dissolved gases | isotope geochemistry | isotope ratio mass spectrometry | nitrogen | noble gases

ABSTRACT

Rationale: The isotopic composition of dissolved dinitrogen gas ($\delta^{15}N\text{-}N_2$) in water can offer a powerful constraint on the sources and pathways of nitrogen cycling in aquatic systems. However, because of the large presence of atmosphere-derived dissolved N_2 in these systems, high-precision (on the order of 0.001‰) measurements of N_2 isotopes paired with inert gas measurements are required to disentangle atmospheric and biogeochemical signals. Additionally, the solubility equilibrium isotope fractionation of N_2 and its temperature and salinity dependence are underconstrained at this level of precision.

Methods: We introduce a new technique for sample collection, processing, and dynamic dual-inlet mass spectrometry allowing for high-precision measurement of $\delta^{15}N\text{-}N_2$ and $\delta(N_2/Ar)$ with simultaneous measurement of $\delta(^{40}Ar/^{36}Ar)$ and $\delta(Kr/N_2)$ in water. We evaluate the reproducibility of this technique and employ it to redetermine the solubility equilibrium isotope effects for dissolved N_2 across a range of temperatures and salinities.

Results: Our technique achieves measurement reproducibility (1σ) for $\delta^{15}N\text{-}N_2$ (0.006‰) and $\delta(N_2/Ar)$ (0.41‰) suitable for tracing biogeochemical nitrogen cycling in aquatic environments. Through a series of air–water equilibration experiments, we find a N_2 solubility equilibrium isotope effect ($\varepsilon = \alpha/1000 - 1$, where $\alpha = (^{29}N_2/^{28}N_2)_{dissolved}/(^{29}N_2/^{28}N_2)_{gas}$) in water of $\varepsilon(‰) = 0.753 - 0.004 \cdot T$ where T is the temperature (°C), with uncertainties on the order of 0.001‰ over the temperature range of ~2°C–23°C and salinity range of ~0–30 psu. We find no apparent dependence of ε on salinity.

Conclusions: Our new method allows for high-precision measurements of the isotopic composition of dissolved N_2 and Ar, and dissolved N_2/Ar and Kr/N_2 ratios, within the same sample. Pairing measurements of N_2 with inert gases facilitates the quantification of excess N_2 from biogeochemical sources and its isotopic composition. This method allows for a wide range of applications in marine, coastal, and freshwater environments to characterize and quantitatively constrain potential nitrogen-cycling sources and pathways and to differentiate between physical and biological isotope signals in these systems.

1 | Introduction

The isotopic composition of nitrogen species in aquatic systems provides insight into nitrogen-cycling pathways, processes, and sources. While isotopic measurements of fixed nitrogen and N_2O are commonly used to constrain biogeochemical cycling, measurements of dissolved N_2 isotope ratios are rare, despite the potential value offered in closing the isotopic

budget of nitrogen in aquatic systems. The dissolved N_2 isotope ratio refers to $\delta^{15}N\text{-}N_2$, which is the deviation of dissolved $^{29}N_2/^{28}N_2$ from the atmospheric ratio. In the ocean and marine sediments, the nitrogen ($^{15}N/^{14}N$) and oxygen ($^{18}O/^{16}O$) isotope ratios of nitrate are measured routinely to constrain the magnitude and rates of nitrogen-transforming processes like nitrification and denitrification [1–3]. Natural nitrogen and oxygen isotopes of nitrous oxide, a potent greenhouse gas, are also measured in marine and terrestrial systems, offering insight into its production and consumption pathways [4, 5]. Measurements of $\delta^{15}N\text{-}N_2$ in the ocean are much less common, owing to small signal-to-noise ratios, and thus have primarily been concentrated in oxygen-poor regions of the ocean exhibiting maximal biogeochemical N_2 generation via denitrification [6–12].

$\delta^{15}N\text{-}N_2$ is more often measured, for example, in rocks where sample sizes are small (on the order of 5–100 μcm^3_{STP} N_2/g [3]), but signals are large (‰ scale) in order to understand the mantle or surface origin of nitrogen [13]. Measurements of $\delta^{15}N\text{-}N_2$ are also common in ice core air bubbles [14, 15], where signals exist at the 0.1‰ scale because of gravitational settling and thermal diffusion. In marine settings, however, detection of meaningful biogeochemical signals requires precision in $\delta^{15}N\text{-}N_2$ well below the order-1‰ scale due to the large contribution of dissolved N_2 inherited from atmosphere–ocean gas exchange. As an example, if all the available nitrate (the dominant form of fixed nitrogen in the ocean) from an average parcel of deep ocean water (nitrate concentration of ~30 μmol/kg) were converted to dissolved N_2 via denitrification, the resultant ~15 μmol/kg of biogenic N_2 would represent only ~2.5% of the background atmosphere-derived N_2 in 2°C and 35 psu seawater at solubility equilibrium with the atmosphere (~593 μmol/kg[16]). As a result, if the $\delta^{15}N$ of biogenic N_2 deviates from the atmosphere at the scale of 10‰ because of a combination of source signals and fractionation mechanisms, the net effect on the total $\delta^{15}N\text{-}N_2$ in seawater would only be 2.5% of this magnitude (i.e., on the order of ~0.1‰). Conversion of fixed nitrogen to N_2 is effectively complete in oxygen minimum zones, but it is thought that excess N_2 from denitrification occurring in particles or sediments may be present throughout a much wider range of the ocean interior [17, 18]. However, with biogenic N_2 representing an even smaller fraction of total N_2 in regions of the ocean where fixed nitrogen removal is incomplete, biogeochemical $\delta^{15}N\text{-}N_2$ signals are suspected to exist at the order-0.01‰ scale, requiring a technique with an analytical uncertainty that is an order of magnitude smaller.

Over the past several decades, advances have been made in the detection of excess N_2 from benthic [8, 18, 19] and water column [20, 21] denitrification. The amount of this excess has been determined in these environments by measuring the ratio of nitrogen to argon, N_2/Ar. Measuring this ratio instead of the abundance of N_2 alone largely removes the effects of physical fractionation due to atmospheric pressure changes at the air–sea interface and cooling during water mass formation of each element, but the ratio is still impacted by air injection at the ocean's surface and in situ N_2 generation by denitrification [18]. Here, we introduce a new method that builds on the N_2/Ar technique by adding high-precision measurements of $\delta^{15}N\text{-}N_2$ and low-precision measurements of Ar isotopes and the Kr/N_2 ratio to better distinguish physical signals (affecting both noble gases and N_2) from biogeochemical signals (only affecting N_2). Our method follows other recent techniques for measurement of $\delta^{15}N\text{-}N_2$ in seawater that have achieved a 1-σ precision of 0.02‰ [10] and 0.01‰ [8], building on these efforts by using a dynamic dual-inlet isotope-ratio mass spectrometer, a hot copper oven to remove oxygen and eliminate associated matrix effects [22, 23], and silica gel beads to trap target gases [24], improving precision to the order-0.001‰ level and eliminating the need for cryogenics or liquid helium for gas processing and transfer. This method is the first to measure $\delta^{15}N\text{-}N_2$ with a bulk gas sample using viscous dual-inlet mass spectrometry while removing O_2, which we believe contributed to our unprecedented precision for these measurements in water.

The capacity to detect small biogeochemical $\delta^{15}N\text{-}N_2$ signals in water demands a need to refine our understanding of N_2 isotopic solubility fractionation (i.e., differences in the solubilities of $^{29}N_2$ and $^{28}N_2$). That is, the $\delta^{15}N\text{-}N_2$ of water deviates from air ($\delta^{15}N\text{-}N_2 = 0$, by definition) because of isotopic solubility differences, and this effect must be known at the order-0.001‰ level for robust quantification of biogeochemical signals. The first experiments to determine the solubility fractionation of N_2 achieved a precision on the scale of 0.1‰ [25]. Two later efforts to constrain the solubility fractionation achieved improved precision of 0.03‰ [26] and 0.02‰ [27], but a comprehensive study at the order-0.001‰ level carried out over a wide range of temperature and salinity remains lacking. In this study, we employed our new method and performed air–water gas exchange experiments to measure the isotopic solubility fractionation of N_2 as a function of temperature and salinity between ~2°C and ~23°C and between ~0 and ~30 psu, respectively. We present an updated N_2 isotope solubility fractionation estimate and discuss its temperature and salinity dependences in the context of recent work to also constrain solubility equilibrium isotope effects (SEIEs) for other gases in water [28–30].

2 | Overview of Analytical Approach

Here, we describe a novel technique for analysis of $\delta^{15}N\text{-}N_2$, $\delta(N_2/Ar)$, $\delta(^{40}Ar/^{36}Ar)$, and $\delta(Kr/N_2)$ in air and water samples. While the sample collection and dissolved gas extraction methods differ between air and water samples (Section 2.1), gas processing using the vacuum purification line (Section 2.2) and mass spectrometry analysis (Section 2.3) are identical for all types of samples. The broad concept underlying this approach is that all samples (air or water) are analyzed via dynamic dual-inlet isotope-ratio mass spectrometry (IRMS) against a common internal reference gas with a water-like (solubility equilibrium) gas composition. By routinely measuring samples of unfractionated atmospheric air, we normalize all measurements to a common external standard: the atmosphere. Formally, for any isotopic or elemental ratio (R; e.g., $^{29}N_2/^{28}N_2$ or N_2/Ar) that is measured, the deviation (δ) of R from the atmosphere is defined as follows:

$$\delta\,(\text{vs. air}) = \frac{R_{smp}}{R_{air}} - 1 = \left(\frac{\left(\frac{R_{smp}}{R_{ref}}\right)}{\left(\frac{R_{air}}{R_{ref}}\right)} - 1 \right) \quad (1)$$

where the subscripts smp, ref, and air refer to sample, internal reference, and air, respectively. In this study, we report δ in per mil (‰). In the following subsections, we describe the protocols for sample collection, processing and transfer, and IRMS analysis.

2.1 | Sample Collection: Air and Water

For water samples, our method implements the dissolved gas sampling technique of Emerson et al. [31] to allow for equilibration of dissolved gases with an evacuated headspace that is subsequently processed and analyzed identically to an air sample. Approximately 300 mL of sample water is collected in an evacuated 500-mL glass flask by continuously flowing water through thin tubing that is inserted in the neck of the flask, which is filled with this flowing water throughout sampling. The valve is slowly opened to carefully allow water to enter without contamination by ambient air. The neck of the flask is filled with CO_2 and capped before and after sampling (Louwers–Hapert double O-ring valves) to minimize leakage of atmospheric air. After collection, sampling flasks spend a minimum of 24 h on a shaker table (Innova 2000 Platform Shaker, 100 rpm) to reach equilibration between the headspace and water at the recorded room temperature. Samples are subsequently inverted and drained into a vacuum chamber, leaving a small amount of water in the flask (~1 mL) to prevent loss of headspace air [31]. Small corrections needed to account for the fractionation of the equilibrated headspace gas relative to the original dissolved gas composition follow Ng et al. [32] and are described in Data S1.

Air samples ($n = 63$) were collected routinely in Woods Hole, Massachusetts, by flushing a two-necked, flow-through, 2-L glass flask (Louwers–Hapert double O-ring valves) for at least 10 min with outside air that has passed through a humidifier (to achieve 100% relative humidity) using a bellows pump at a flow rate of ~4 L min^{-1}. Aliquots were then taken for sampling (~4 mL) by opening the flask to a fixed volume on the vacuum purification line after attaching the flask, pumping down the connection, and leak checking. An ultimate gas sample size on the order of 1 mL (whether air or dissolved gas) is needed to maintain balanced, viscous flow (> 20 mbar pressure) in the dual inlet of the mass spectrometer without the need for an added carrier gas.

In this study, we evaluate our analytical technique using a set of air–water equilibration samples ($n = 35$) collected for the purpose of determining the SEIEs of N_2 in water. The freshwater samples in this study were collected using the air-equilibrated water chamber described in Jenkins et al. [33]: a temperature-controlled setup containing a glass chamber (4.75-L sample volume; filled approximately 3.5 L with deionized water collected from a Milli-Q system), a humidifier through which outside air flows before flowing through the system's headspace, and temperature and pressure probes. A magnetic stir bar in the bottom of the glass chamber was set to rotate at a rate of 600 rpm, allowing for mixing without introduction of bubbles. The rate of outside air flowing through the humidifier and headspace of the system was ~20 mL min^{-1}, resulting in a flushing of the headspace approximately every 60 min. The water equilibrated with this setup for a minimum of 72 h before sampling. Saltwater samples were collected in an equilibration chamber (14-L sample volume; filled with approximately 10 L of UV-sterilized seawater) at room temperature. The chamber headspace was first flushed with outside air continuously for 24 h, then closed off and allowed to equilibrate (as a closed system) for at least 3 days while stirring with a magnetic stir bar (at ~400 rpm) before collecting samples. Two separate batches of saltwater equilibration experiments were carried out.

2.2 | Gas Processing and Transfer

Gas samples—either air or headspace gases of drained water samples—were processed on a custom vacuum system (Figure 1) in the Seltzer Laboratory at Woods Hole Oceanographic Institution (WHOI). The aim of sample processing is (i) to isolate target gases (N_2, Ar, and Kr) in a sample by removing any potentially interfering gases (O_2, CO_2, and water vapor) during mass spectrometry and (ii) to quantitatively transfer these target gases into a dual-valve dip tube that is subsequently removed and connected to an IRMS for measurement (Section 2.3). Our technique uses a hot furnace (~500°C) filled with copper turnings for quantitative removal of O_2, similar to previously described methods [22, 23]. Removal of O_2 is critical because interaction between N_2 and O_2 in the IRMS ion source leads to an apparent bias (i.e., "matrix effect" [15, 24, 34]) in $\delta^{15}N\text{-}N_2$ that scales with the amount of oxygen in the sample, with a sensitivity on the order of 0.0001‰ (for $\delta^{15}N\text{-}N_2$) per 1‰ change in the O_2/N_2 ratio (see Figure S2, which shows the results of an experiment in which O_2 is progressively added to a reference gas to assess the bias in $\delta^{15}N\text{-}N_2$). Because the method is designed intentionally to robustly measure $\delta^{15}N\text{-}N_2$ in air and water, and the solubility equilibrium ratio of O_2/N_2 is roughly twice that of air [16] (i.e., a ~1000‰ difference in O_2/N_2), the bias in $\delta^{15}N\text{-}N_2$ due to the presence of O_2 (i.e., the O_2 matrix effect) in an air-like sample relative to a water-like reference gas would be on the order of 0.1‰, requiring a correction that is larger in magnitude than expected biogeochemical signals in aquatic systems (Figure S2). For this reason, we opted to quantitatively remove > 99.9% of O_2 from all samples to eliminate any O_2 matrix effect on $\delta^{15}N\text{-}N_2$ at the order-0.001‰ level. Our method involves the capture and transfer of N_2, Ar, and Kr without the need for a cryostat or liquid helium, which is often expensive and may become more difficult to acquire because of dwindling global helium reserves. Silica gel is inexpensive and relatively easy to obtain, and cryosorption of the target gases in this study is feasible using liquid nitrogen (−196°C) for cooling. Our approach builds on recent work demonstrating the suitability of silica gel for the transfer of heavy noble gases for high-precision dynamic IRMS analysis [24].

The custom vacuum line used in this study (Figure 1) includes bellows-sealed valves, various pressure gauges, two water traps, a copper furnace, and a detachable dual-valve dip tube. A Pfeiffer HiPace 80 turbomolecular pump is used to attain and maintain high vacuum ($< 10^{-4}$ Torr), backed by an Edwards nXDS 6i scroll pump. The glass traps are both custom Ace Glass components (shortened versions of model 8670). The first trap is submerged in an ethanol–liquid N_2 slurry (−95°C to −105°C) to remove water vapor, while the second trap is submerged only in liquid N_2 (−196°C) to remove

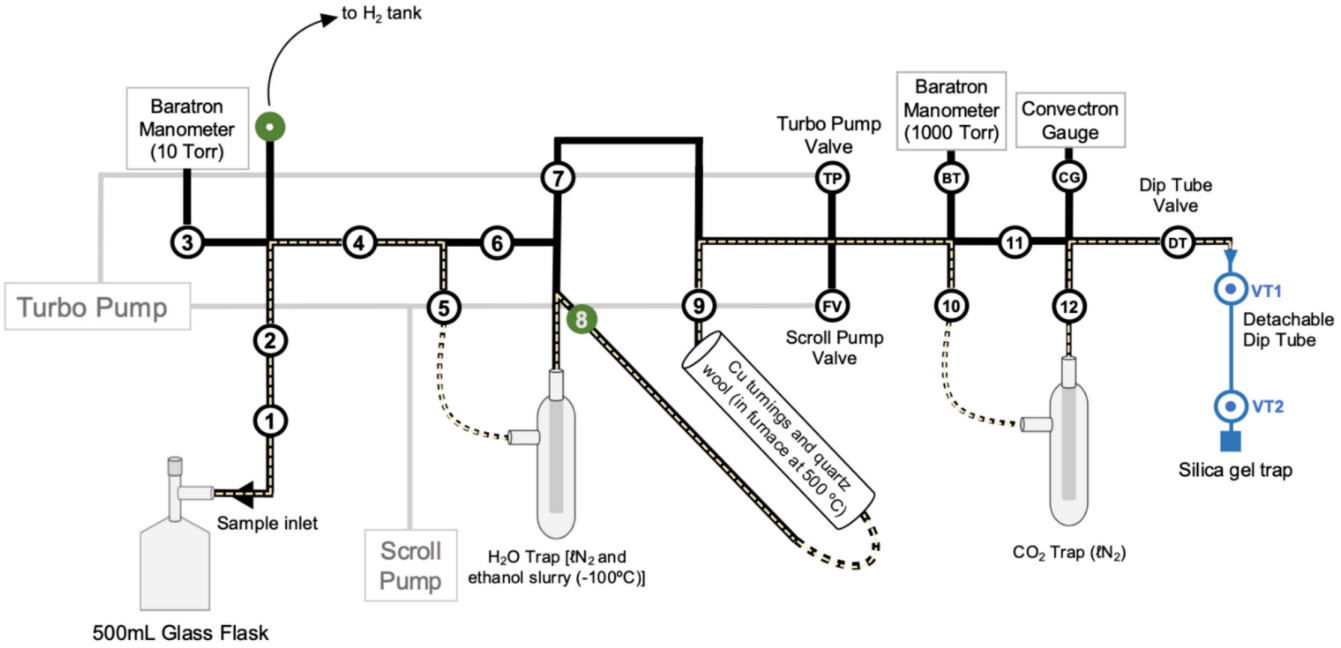

FIGURE 1 | Schematic of the vacuum line used for sample extraction of both air and dissolved gas samples in this study. Labeled circles represent valves (black: Swagelok SS-4BG and green: Swagelok SS-4H). Dip tube (colored blue) is detachable from the line to transfer purified gas to IRMS for analysis. Yellow dashed lines represent the intended gas flow path through the vacuum line.

CO_2. The temperature of the ethanol–liquid N_2 slurry is monitored throughout the extraction, and more liquid N_2 is added as needed to maintain the correct temperature. We note that an early trial of the method in which both water traps were cooled by liquid N_2 was abandoned due to an observed physical fractionation associated with adsorption of N_2, Ar, and Kr onto ice at −196°C that formed in the first water trap when processing water samples. The copper furnace is 1/2″ diameter quartz tubing approximately 9″ in length containing copper shavings (through 4″ of tube) bookended by quartz wool (~1″ of tube, each side), both of which have been cleaned by sonication in acetone. The entirety of the copper is arranged inside a ceramic cylinder heater (Watlow VC400N06A) connected to a variable transformer, allowing heating to 500°C for routine sample processing, and to at least 750°C to "bake out" the copper before the first use or after exposure to ambient air to ensure that any adsorbed contaminants are fully removed. Two MKS Baratron capacitance manometers (10 and 1000 Torr) are used to monitor sample pressure after expansion into the vacuum line and the pressure of the hydrogen gas used to regenerate the copper. A Granville–Phillips 275 Convectron gauge is used both for leak testing prior to sample processing and for monitoring the effective pressure of the sample when flowing through the copper furnace. Target gases are transferred from the vacuum purification line to the IRMS via detachable dip tubes, which have two Swagelok 4BG bellows-sealed valves separating a stainless-steel chamber (~10 mL) from a smaller chamber (~1 mL) filled with 36 variably sized silica gel granules.

During processing, sample gas initially travels from either the air aliquoting volume (between Valves 1 and 2) or the drained water sampling flask (with Valves 1 and 2 open; Figure 1). After the sample and dip tube are connected, the line is pumped to high vacuum and leak checked by closing the turbomolecular pump valve (TP), which isolates the line from the pump. The first water trap is cooled by an ethanol–liquid N_2 slurry, monitored regularly to ensure that the temperature remains within the range from −95°C to −105°C, while the second water trap is immersed in liquid N_2. Once the line is pumped down and water traps cooled, a leak test is performed with a passing threshold of less than a 10^{-4} Torr rise in pressure over a 2-min period. After passing a leak check, Valves 8 and 9 are closed to isolate the Cu furnace, which starts heating to 500°C while other sample preparations occur. In the case of an air standard, Valve 2 is closed and Valve 1 is opened, and the 2-L air flask is allowed to expand into the line to Valve 2 and equilibrate for 10 min (extracted dissolved gas samples have already been equilibrated and drained, so no further equilibration step is necessary). Next, the valve closest to the line on the dip tube (VT1) is opened, and the silica gel trap is heated to 200°C with heating tape for 3 min to remove any possible adsorbed gases left over from the prior measurement. This is in addition to the silica gel beads in the dip tube being pumped for a minimum of 1 h on the mass spectrometer inlet after IRMS analysis and before reusing the tube to process the next sample.

After cooling and passing a second leak check with the same stipulations as the first leak check, VT1 is closed. The portion of the dip tube containing the silica gel trap (i.e., below Valve VT2) is then submerged in liquid N_2 for the remainder of sample processing. Valve 9 is reopened, and once the Cu furnace has reached 500°C, a third and final leak test is performed with the same passable rate, to ensure that no contaminants are being released from the copper turnings (or, at a minimum, that no contaminants persist past the second water trap). At this point, sample processing is ready to begin, and Valves 6–8, 11, TP, and FV are closed (as is Valve 1 in the case of an air measurement), and Valves 2 and VT1 are opened. Valve VT2 remains open the entire time. To begin the

flow of gas, either Valve 2 (air sample) or the 500-mL flask valve (extracted dissolved gas sample) is opened. The sample expands into the left half of the line and is able to flow through the first water trap but is trapped by Valves 7 and 8. Valve 8 is a Swagelok SS-4H bellows-sealed valve that is gradually opened at this point to allow gas to pass through into the copper furnace. To ensure sufficiently low pressure (and a correspondingly long mean free path) for the maximum interaction between gases and the hot copper, the valve is opened only until the convectron pressure reads 250×10^{-3} Torr. This pressure is maintained over time by opening Valve 8 gradually until fully opened, and the pressure begins to decrease as the sample gas upstream of the furnace is depleted and the gas downstream is trapped cryogenically on the cold silica gel in the dip tube. After fully opening the valve, sample processing continues for 40 min to ensure quantitative transfer of gas into the dip tube (Figure S3), with trap temperatures monitored and dewars refilled as needed. After 40 min, Valve VT1 is closed, and the tube is removed from the line and connected to the inlet of the IRMS.

To regenerate the copper furnace so it can be used to remove O_2 in the next sample, H_2 gas flows through the hot furnace (pumped by the scroll pump) for a period of 10 min with sufficient flow rate, maintaining a measured pressure on the convectron readout of at least 300×10^{-3} Torr (equivalent to 250×10^{-3} Torr of hydrogen gas on a N_2-calibrated convectron) [35]. On the IRMS inlet, the dip tube sits at room temperature for a minimum of 3 h to allow for desorption and diffusive equilibration within the tube. After equilibration and before analysis, Valve VT2 is closed, isolating the purified gas from the silica gel for IRMS analysis. This isolation is critical to ensure that any slight fraction of sample gas remaining adsorbed to the silica gel at equilibrium does not desorb upon expansion of sample gas into the IRMS bellows, as prior work has shown that desorption-induced kinetic fractionation can be substantial [24]. In total, accounting for sample processing, transfer, tube equilibration, and mass spectrometry analysis, it takes approximately 5.5 h to run one sample. Notably, because the processing line is decoupled from the mass spectrometer, purification and transfer of one sample can occur while another is equilibrating or being analyzed, allowing for the processing of two to three samples in a standard workday.

2.3 | Dynamic Isotope-Ratio Mass Spectrometry Analysis

Processed gas samples are analyzed on a refurbished Thermo MAT 253 dual-inlet IRMS in the Seltzer Laboratory at WHOI. Because this instrument has a collector array originally designed for other purposes, analysis of N_2, Ar, and Kr is carried out by magnetic peak jumping between three gas configurations. After sample analysis, we implement a final set of peak jumps to gas configurations for CO_2 and O_2 to check that these potentially interfering gases (via matrix effects) are sufficiently low in abundance. All samples are analyzed against a common reference gas (Can 1), which is a 2-L stainless steel can with a roughly 1-mL aliquoting chamber, filled to ~2000 Torr. Can 1 contains a N_2–Ar–Kr admixture in approximately air-equilibrated water-like gas ratios without O_2 due to the aforementioned "matrix effects" on the IRMS O_2 causes. We occasionally test for instrumental drift by measuring an aliquot of gas from a secondary reference can (Can 2) with similar dimensions and pressure but an air-like composition of N_2, Ar, and Kr.

Our IRMS analysis approach broadly follows other similar dual-inlet IRMS methods for measuring N_2 isotopes [14, 34, 36], with a key difference being that we analyze samples either with air-like or water-like N_2–Ar–Kr composition, while prior studies exclusively analyzed air-like samples against an air-like reference gas. This distinction has substantial practical importance because the elemental ratios of N_2/Ar and Kr/N_2 vary substantially between air and air-equilibrated water samples [16, 33], meaning that the automatic compression of sample and reference bellows to achieve the same Ar and Kr ion beam intensities could result in extremely imbalanced pressures, violating a key requirement of dynamic IRMS analysis. To accommodate both air and air-equilibrated water samples while adhering to the fundamental requirement of balanced pressure in both sample and reference bellows, we set the pressure in each bellows by automatically compressing to achieve a $^{28}N_2^+$ ion beam intensity of 10 V (on a Faraday cup amplified by a $3 \times 10^8\ \Omega$ resistor). This corresponds to a pressure of ~85 mbar for an air sample in each bellows. Because Kr is a trace gas and Ar represents ~1% of the total gas in an air sample and ~2% of the total gas in a water sample, this approach ensures that the pressure is balanced between the sample and reference bellows to within ~1% at all times for the analysis of every sample, independent of its composition. This N_2-balancing approach is analogous to the use of ^{40}Ar for pressure balancing for samples of widely variable heavy noble gas composition in the method of Seltzer and Bekaert [24].

Prior to analysis, a leak check is performed before an aliquot from Can 1 is collected by equilibrating with the inner can valve open and outer valve closed for 10 min. Once the reference gas equilibration is complete, the sample and reference aliquots are introduced into their respective bellows, equilibrating again for 10 min before the bellows are isolated and the measurement sequence is started. A typical analysis includes three "blocks" of N_2–Ar measurements in which

i. peak centering is performed,
ii. pressure balancing is achieved by compressing both bellows to reach 10-V ion beam intensity for $^{28}N_2^+$,
iii. four integration cycles of N_2 isotope analysis are completed (20-s integration and 8-s idle time), alternating between sample and reference bellows,
iv. magnetic peak jumping is carried out to reach the Ar gas configuration,
v. peak centering is performed,
vi. three sample-reference integration cycles are completed (20-s integration and 8-s idle time), and
vii. magnetic peak jumping back to the N_2 gas configuration is carried out, and four more N_2 integration cycles are completed.
i. briefly peak centering and pressure balancing on $^{28}N_2^+$ and completing a single N_2 integration cycle,

ii. peak jumping to the Kr gas configuration, peak centering, and carrying out five sample-reference integration cycles in which $^{84}Kr^+$ is measured (20-s integration time and 15-s idle time), and

iii. peak jumping back to N_2, peak centering, and completing a single N_2 integration cycle.

After measuring N_2 ($^{28}N_2$ and $^{29}N_2$) and Ar (^{36}Ar and ^{40}Ar), three blocks of Kr analysis are carried out by the following:

The average $^{28}N_2^+$ and $^{40}Ar^+$ beam intensities over an N_2–Ar block are then used to calculate $\delta(N_2/Ar)$ (or the average $^{28}N_2^+$ and $^{84}Kr^+$ beam intensities over a Kr–N_2 block to calculate $\delta(Kr/N_2)$). Similarly, the average of individual-cycle $\delta^{15}N\text{-}N_2$ and $\delta(^{40}Ar/^{36}Ar)$ across each block is used to calculate the block mean δ values for these ratios. For each sample, we correct for pressure imbalance sensitivity (PIS) for each block by using the apparent PIS for each sample, which on this particular IRMS is a negligible correction in most cases. This correction is made in the same way as in prior studies [24, 34]. We define pressure imbalance (PI, in per mil) as the fractional deviation of sample and reference $^{28}N_2^+$ beam intensities averaged across a measurement block and compute PIS by regressing block-mean δ values against block-mean PI values. Across all measurements in this study, the average PIS for $\delta^{15}N\text{-}N_2$ was -7.9×10^{-5}‰‰$^{-1}$, and the average sample-mean absolute PI was 8.8‰, leading to a mean PIS correction for $\delta^{15}N\text{-}N_2$ of less than 0.001‰. For other ratios measured, the mean PIS corrections were similarly below the 1-σ precision of the measurement.

All measured ratios were also corrected for matrix effects (ME; also sometimes referred to as "chemical slopes"), whereby differences in the bulk composition of sample and reference gas lead to apparent biases in measured ratios due to a wide range of processes, including ion–ion interaction, space charge effects in the ion source, and, in the case of imbalanced elemental ratios, instrumental nonlinearity. As an example, for measurement of a sample gas with an air-like N_2/Ar ratio against the common reference gas with a water-like elemental composition (Can 1), we must correct for biases in the isotopic and elemental ratios that arise both from ion source effects and from nonlinearity. This is due to the fact that Ar and Kr ion beams are much larger in the water-like reference gas than in an air-like sample. Following Seltzer and Bekaert [24], we correct for elemental ratio and Ar isotope ratio matrix effects by assuming that any apparent biases in measured $\delta(N_2/Ar)$, $\delta(Kr/N_2)$, and $\delta(^{40}Ar/^{36}Ar)$ in air-equilibrated water samples, relative to expected values from published solubility functions [16, 30, 33], are due to ratio-specific ME. We then correct for these effects in all samples by using optimal ME values from least-squares minimization of measured values applied to known solubility equilibrium values.

For example, PIS-corrected $\delta(^{40}Ar/^{36}Ar)$ is corrected for ME by subtracting ME × $\delta(N_2/Ar)$, where ME is the optimal ME value for $^{40}Ar/^{36}Ar$ based on the minimization of deviations in measured PIS-corrected $\delta(^{40}Ar/^{36}Ar)$ in air–water equilibration experiments from published solubility equilibrium values. We find optimal ME values for N_2/Ar, Kr/N_2, and $^{40}Ar/^{36}Ar$ of 0.0064‰‰$^{-1}$, −0.0003‰‰$^{-1}$, and −0.0088‰‰$^{-1}$, respectively. The apparent ME for $^{40}Ar/^{36}Ar$ is of the same sign and approximate magnitude as that found by Severinghaus et al. [34] using a Finnigan MAT 252 mass spectrometer (−0.0010‰‰$^{-1}$). The ME correction for elemental ratios is made following the framework of Seltzer and Bekaert [24], and while the N_2/Ar optimal ME results in a very small correction, the Kr/N_2 correction is more appreciable, in line with the results from two recent studies carried out using different IRMS instruments that found ‰-to-%-scale ME corrections were required based on air-equilibrated water measurements of Kr/Ar and Xe/Ar ratios [24, 32]. Because the solubility equilibrium isotopic composition of N_2 was not known to sufficient precision prior to this work, the method of minimizing deviations between measured and published solubility functions was not possible to determine ME for $\delta^{15}N\text{-}N_2$.

Because N_2 is the dominant gas and our method allows for pressure balancing to within ~1% independent of elemental composition, we expected that, by design, the method should be insensitive to any apparent N_2 isotope ME. However, because Ar concentration varies between ~1% and 2% of the total gas in purified air and water samples in this study (Kr is a trace gas, representing <0.001% of the total gas in both air and water samples), we carried out an experiment to determine if there was an appreciable ME over the N_2/Ar range of air and water samples. We added increasing amounts of argon to aliquots of gas collected from our secondary reference can (Can 2, air-like elemental composition) to increase the Ar/N_2 ratio up to and beyond that of air-equilibrated water. Each aliquot was transferred onto the silica gel in a dip tube and analyzed like a normal sample. Across these experiments, we find a very slight but clearly discernible and linear ME, with an optimal value of 1.5×10^{-5}‰‰$^{-1}$ (Figure 2). Thus, in all samples, we corrected for N_2 ME by subtracting the optimal ME values × PIS-corrected $\delta(Ar/N_2)$ value (reported against Can 1). Across the range of air-like to water-like Ar/N_2 ratios, this results in a maximum ~0.007‰ correction to $\delta^{15}N\text{-}N_2$, a small but important correction given that it

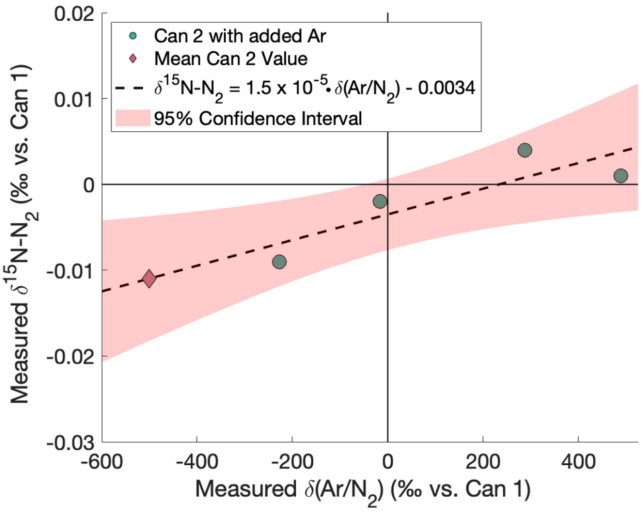

FIGURE 2 | Matrix effect slope determined for $\delta^{15}N\text{-}N_2$ due to the presence of Ar. Progressively larger quantities of pure Ar were added to aliquots from standard Can 2 (air-like N_2–Ar–Kr elemental composition), transferred onto the detachable dip tubes, and analyzed against the common reference gas (Can 1; water-like N_2–Ar–Kr elemental composition).

TABLE 1 | Summary of air–water equilibration experiments.

Experiment information				Experiment-mean values (‰ vs. air)			
ID	# samples	Temp (°C)	Sal (psu)	$\delta^{15}N\text{-}N_2$	$\delta(N_2/Ar)$	$\delta(^{40}Ar/^{36}Ar)$	$\delta(Kr/N_2)$
4	5	1.98	0.0	0.737	−553.476	1.052	3579.682
3	4	8.22	0.0	0.722	−548.755	1.159	3360.092
2	6	12.2	0.0	0.714	−545.584	1.131	3231.668
1	6	16.1	0.0	0.687	−542.316	1.047	3122.129
7	5	20.0	0.0	0.676	−538.672	1.047	2986.541
6	5	22.3	30.3	0.665	−544.274	1.010	2965.833
5	4	23.0	30.0	0.648	−543.495	0.927	2947.934

is slightly larger than the 1-σ measurement uncertainty of water samples in this study.

3 | Evaluation of the Analytical Method

3.1 | Overall Reproducibility of Air and Water Measurements

A total of 63 aliquots of atmospheric air (~4 mL in size) were analyzed routinely between July and December 2024. Two dip tubes were used in this study (Tubes C and E), each with 36 granules of silica gel. However, because of small variability in the size of silica gel granules, the effective volumetric ratio of silica gel to gas headspace in each tube differed slightly, likely leading to small but significant observed offsets between the two tubes due to the slight amount of fractionated N_2 and Ar that remains adsorbed to silica gel after equilibration. For example, across all air measurements ($n = 35$ for Tube C; $n = 28$ for Tube E), we observed mean $\delta(N_2/Ar)$ (±1 SE) of 1152.675‰ ± 0.063‰ for Tube C and 1151.895‰ ± 0.120‰ for Tube E, reported relative to internal reference Can 1 (water-like composition). The observed tube offsets in mean $\delta^{15}N\text{-}N_2$, however, were not statistically significant, with mean values (±1 SE) of 0.439‰ ± 0.002‰ for Tube C and 0.442‰ ± 0.002‰ for Tube E, reported relative to Can 1, indicating that tube differences in equilibrium adsorption have minimal impact on N_2 isotopes. All water samples in this study were normalized to air via Equation (1), using the mean values of all air measurements from the particular dip tube that was used for the water sample. In this way, any slight tube-specific fractionation due to equilibrium adsorption on silica gel is common to both air and water samples and therefore cancels in Equation (1). A total of seven air–water equilibration experiments were carried out in this study with multiple samples collected from each experiment, leading to a total of 35 water measurements. The details of each experiment, including the equilibration temperature, salinity, number of samples measured, and mean isotope ratios (normalized to air), are provided in Table 1. Two separate batches of saline samples (~30 psu salinity, total of nine samples) were taken and measured during this study. A full summary of all individual air and water measurements is included in Data S1.

To evaluate the reproducibility of air and water measurements, we compute the pooled standard deviation of (a) air samples measured relative to internal reference Can 1 and (b) air-equilibrated water samples reported relative to atmospheric air after tube-specific normalization. To compute the pooled standard deviations, we first determine sample-specific anomalies δ′ for all individual measurements (δ_{smp}) relative to the group-mean value ($\overline{\delta_{group}}$), where the group is either (a) all air samples processed using a particular dip tube (i.e., either Tube C or Tube E) or (b) all water samples from a particular experiment:

$$\delta'(\text{vs. group mean}) = \left(\frac{\delta_{smp} + 1}{\overline{\delta_{group}} + 1} - 1\right) \quad (2)$$

The pooled standard deviation (σ_{pld}) is then computed separately for air and water samples as follows:

$$\sigma_{pld} = \sqrt{\frac{\sum(\delta')^2}{N - k}} \quad (3)$$

where N is the total number of samples measured (i.e., 63 for air and 35 for water) and k is the total number of groups (i.e., 2 for air [Tubes C and E means] and 7 for water [the 7 experiments listed in Table 1]). The resulting σ_{pld} values serve as useful indications of the overall reproducibility of measured ratios in air and water. These values are reported in Table 2, and δ′ values of this calculation are provided in Data S1. Given that air-equilibrated water has higher Ar/N_2 and Kr/N_2 than air, the higher precision (lower σ_{pld}) observed for $\delta(Kr/N_2)$ and $\delta(^{40}Ar/^{36}Ar)$ in water relative to air likely results from the fact that Ar and Kr beam intensities are higher in water samples than in air samples. It is not immediately clear why the precision of $\delta^{15}N\text{-}N_2$ is higher in water, but the precision of $\delta(N_2/Ar)$ is higher in air. Nonetheless, the observed

TABLE 2 | Pooled standard deviations of all air ($n = 63$) and water ($n = 35$) samples in this study.

Sample type	Pooled standard deviation, σ_{pld} (‰)			
	$\delta^{15}N\text{-}N_2$	$\delta(N_2/Ar)$	$\delta(^{40}Ar/^{36}Ar)$	$\delta(Kr/N_2)$
Water	0.006	0.41	0.070	2.3
Air	0.009	0.24	0.161	5.3

precision of $\delta^{15}N\text{-}N_2$ in water exceeds that of any existing study, to our knowledge, and the observed precision of $\delta(N_2/Ar)$ is similar to other dynamic IRMS studies. For example, our $\delta(N_2/Ar)$ σ_{pld} value for water (0.41‰) is comparable to the reported 0.68‰ pooled standard deviation of duplicate samples by Hamme and Emerson [18]. The precision of Ar isotopes is roughly 10 times lower (i.e., $\sigma_{pld}=0.07$‰) than a recent high-precision technique [24], but our sample size (~300 mL) is similarly roughly 10 times smaller than that study (~3.5 L). Additionally, the design of our IRMS measurement sequence prioritizes N_2 isotopes, carrying out a total of only nine integration cycles for Ar isotopes. If needed for future applications, the precision of Ar isotope measurements could likely be enhanced through the extension of the sample run time to add more integration cycles of Ar. However, in practice, it is often feasible to collect separate samples for analysis using our method (prioritizing N_2) and the heavy noble gas-focused method [24]; thus, the duplication of Ar isotope measurements serves as a useful internal consistency check. Finally, the reproducibility of Kr/N_2 in this study ($\sigma_{pld}=2.3$‰) is similar to the ~2‰ reproducibility of dissolved Kr abundance measurements in the method of Jenkins et al. [33] and close to the ~1‰ 1-σ reproducibility of Kr/Ar ratios measured via the method of Seltzer and Bekaert [24].

3.2 | Sensitivity to Headspace–Water Equilibration Time and Temperature

To evaluate the potential for bias in measured $\delta^{15}N\text{-}N_2$ using our dissolved gas technique, we explore apparent sensitivities to leakage across Viton O-rings, incomplete dissolved gas–headspace equilibration, and variations in laboratory temperature during headspace equilibration. In Figure 3, we compare water sample $\delta^{15}N\text{-}N_2$ anomalies, δ' (see Section 3.1), to headspace equilibration time and laboratory temperature measured at the end of the equilibration. We find no statistically significant trend in δ' with respect to equilibration time or temperature for $\delta^{15}N\text{-}N_2$ or any other three ratios measured in this study (Figures S4–S6). The lack of a dependence of δ' on equilibration time suggests that (a) 24 h is a sufficient period of time for complete equilibration, and

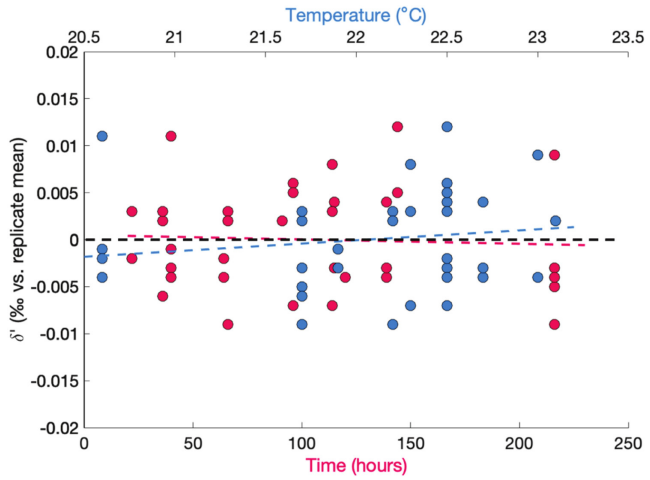

FIGURE 3 | Sensitivity of $\delta^{15}N\text{-}N_2$ to headspace-dissolved gas equilibration time (in pink) and temperature (in blue). Shown here are sample anomalies, δ', relative to experiment-mean $\delta^{15}N\text{-}N_2$ values for all water samples in this study ($n=35$).

(b) over the maximum period of equilibration (~17 days), there is no appreciable fractionation due to leakage of air into the flask. Any detectable leakage of air into the low-pressure flask would cause significant kinetic isotope fractionation that would give an anomalously low isotopic value for $\delta^{15}N\text{-}N_2$. Given that Ar and N_2 have been shown to permeate slowly through Viton O-rings [37], this analysis also provides important evidence that our method, which includes the use of CO_2 as a buffer gas in the sample neck before sampling and during headspace equilibration, prevents any appreciable leakage of atmospheric air into samples over the timescale of weeks, at minimum. Our method of sampling and storage is similar to other established techniques [31, 38], which have also used a CO_2 capping method to prevent leaks between sampling in the field and measurement in the lab. An additional storage consideration is to avoid prolonged exposure to sunlight prior to sample draining, as a recent study showed that N_2O can be produced photochemically in marine and fresh waters [39]. Similarly, the insensitivity of our measurements to laboratory equilibration temperature, which varied by ~2.5°C over the full set of samples, suggests that our headspace-dissolved gas solubility correction (outlined in detail in Data S1), which accounts for temperature measured at the end of equilibration, is robust at the level of precision of our measurements.

3.3 | Silica Gel Fractionation Effects

As detailed in Section 3.1, because air standards and air-equilibrated water samples are analyzed in the same two dip tubes against a common internal reference gas (Can 1), the normalization of measured gas ratios in water samples to the mean of air standard measurements cancels out any potential fractionation due to equilibrium adsorption on silica gel within the dip tubes. Nonetheless, for completeness, we evaluate the extent to which equilibrium adsorption on silica gel beads may fractionate the main gas ratios of interest in this study.

To perform this evaluation, we analyzed a secondary reference gas (Can 2, with air-like elemental composition) against Can 1 (water-like elemental composition) in two ways. For one technique, we introduced aliquots of gas from both cans directly to their respective bellows in the IRMS dual-inlet system. In the other, we transferred aliquots of Can 2 into sample dip tubes (using ethanol and liquid N_2 to trap gases, like a typical sample) and then analyzed against Can 1 after equilibration in the dip tube and isolation of the sample gas from silica gel by closing Valve VT2 prior to analysis, as is done for a typical sample. We refer to measurement using the first approach as "direct" and the second as "silica gel tube" measurements.

Figure 4 shows the results of this analysis, with measured values reported against the internal reference gas (Can 1). We find no statistically significant difference between the means of direct ($n=20$) and silica gel tube ($n=4$) $\delta^{15}N\text{-}N_2$ measurements (−0.009‰ ± 0.002‰ and −0.011‰ ± 0.003‰, respectively; ±1 SE). However, we find that the mean $\delta(N_2/Ar)$ of silica gel tube measurements (1003.476‰ ± 0.212‰; ±1 SE) falls below the mean $\delta(N_2/Ar)$ of direct Can 2 measurements (1010.258‰ ± 0.303‰; ±1 SE), demonstrating that slightly more N_2 than Ar remains adsorbed to silica gel at equilibrium. Note that these $\delta(N_2/Ar)$ values are high because of the air-like elemental composition of Can 2, and because addition and

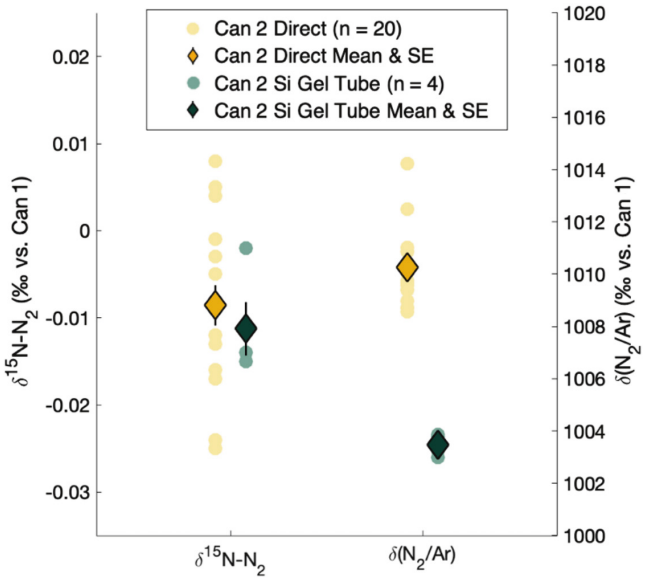

FIGURE 4 | Direct and silica gel tube $\delta^{15}N\text{-}N_2$ and $\delta(N_2/Ar)$ measurements of reference Can 2 (air-like elemental composition) against internal reference Can 1 (water-like elemental composition) (see Equation 4 for determination of difference in absorption seen in $\delta(N_2/Ar)$, accounting for the non-exact additivity of δ values).

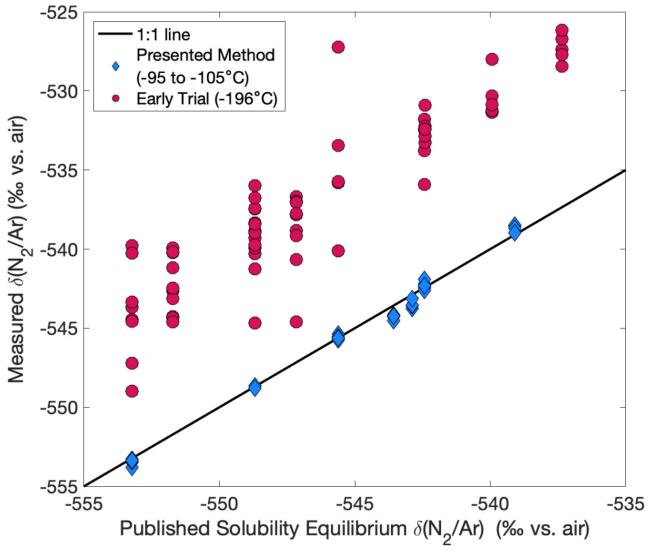

FIGURE 5 | Comparison of measured $\delta(N_2/Ar)$ to published solubility equilibrium of $\delta(N_2/Ar)$ in air–water equilibration experiments carried out using an early trial of the method (red circles) and the presented version of the method (blue diamonds). The early version used liquid N_2 (−196°C) to cool the water trap, whereas the presented version of the method used an ethanol–liquid N_2 slurry (−95°C to −105°C). The published solubility equilibrium values come from Hamme and Emerson [16].

subtraction of δ are only good approximations for small values, the apparent fractionation of N_2/Ar ($\varepsilon_{Si\text{-}Gel}$) due to adsorption on silica gel must be calculated by normalizing the silica gel tube measurements of Can 2 to direct measurements of Can 2:

$$\varepsilon_{Si-Gel} = \frac{\delta_{Si-Gel-Tube} + 1}{\delta_{direct} + 1} - 1 \quad (4)$$

We find an apparent ε_{Si-Gel} of −3.4‰ for N_2/Ar, indicating that, if ~100% of Ar is released from silica gel at room temperature [24], ~99.7% of N_2 is released. The lack of fractionation between direct and silica gel tube experiments for $\delta^{15}N\text{-}N_2$ indicates that this small fraction of N_2 left adsorbed at equilibrium does not lead to substantial enough fractionation to detect at the level of precision of our method. Repeating this exercise for Kr/Ar, we find an apparent ε_{Si-Gel} of −77.4‰, which is larger than the approximately −28.0‰ Kr/Ar fractionation reported by Seltzer and Bekaert [24] because of silica gel dip tube equilibration. We suspect that the larger Kr/Ar fractionation reported in this study likely results from a combination of (a) the use of more silica gel in the dip tube (36 granules instead of 10) and (b) equilibration at room temperature instead of at 30°C, as was done in the method of Seltzer and Bekaert [24].

3.4 | Sensitivity to Water Trap Temperature

All data presented in this study were analyzed using the version of the method described previously. For completeness, and to inform readers who may have interest in replicating and/or modifying our method, here we briefly describe results from an early trial of the method that was used in a separate series of air–water equilibration traps. In this early method trial, the borosilicate glass water trap (Figure 1) was held at −196°C by a liquid N_2-filled dewar during sample processing, instead of being held between −95°C and −105°C by an ethanol–liquid N_2 slurry. In these experiments, which were carried out using freshwater equilibrated at temperatures between 2°C and 19°C, we observed much poorer overall reproducibility and a systematic bias in $\delta(N_2/Ar)$, $\delta(^{40}Ar/^{36}Ar)$, and $\delta(Kr/N_2)$, although no bias in $\delta^{15}N\text{-}N_2$ (Figure S8). For example, Figure 5 shows a comparison between measured $\delta(N_2/Ar)$ and published solubility equilibrium $\delta(N_2/Ar)$ from Hamme and Emerson [16] in both the early trial and the presented methods. We find that the σ_{pld} for $\delta(N_2/Ar)$ of the early method is an order of magnitude larger than the presented method (4.84‰ vs. 0.24‰), and the mean $\delta(N_2/Ar)$ is ~10‰ higher (when δ is reported with respect to air). Note that the non-exact additivity of δ suppresses this difference because $\delta(N_2/Ar)$ is far from zero (N_2/Ar in water is roughly half that of air), so that the net effect (calculated analogously to the calculation involving Equation 4 in the previous section) is a positive bias in N_2/Ar of 22.2‰. We also observe a much greater reduction in precision for Kr/N_2, accompanied by a large and variable low bias in data analyzed using the early liquid-N_2 cooled water trap method (Figure S7). A full summary of these analyses using the early method, along with a calculation of the pooled standard deviations of measured gas ratios, is provided in Data S1.

We suspect that the origin of the strong biases and large variability in water samples analyzed using the early liquid N_2 trial of the method stems from the adsorption of gases onto ice crystals that form in the water trap during analysis. Several clues in the dataset support this hypothesis. First, the observed biases in the liquid N_2 version of the method include a reduction of Kr/Ar and an increase in N_2/Ar. Of these three gases, Kr has the highest boiling point and N_2 the lowest. While it has been demonstrated previously that liquid N_2 does not remove Kr at low pressure in glass traps during vacuum line processing [34] despite the

boiling point of Kr being above the temperature of liquid N_2, the formation of ice in the trap may provide sites for cryosorption. If so, one might expect that Kr would be most affected (owing to its high boiling point), followed by Ar, and then N_2, which would lead to a reduction of the Kr/N_2 ratio and an increase in the N_2/Ar ratio of gas that manages to pass through the trap, consistent with our findings. Second, the lack of appreciable N_2 isotope fractionation is consistent with the notion that the adsorption of N_2 onto ice is minimal and/or the isotope effect associated with adsorption is small, which is supported by our finding of no significant fractionation associated with N_2 adsorption on silica gel (Section 3.3). Third, the reduction in precision may stem from slight sample-to-sample differences in adsorption and desorption driven by variations in the timing of the complete opening of Valve 8 (exposing sample gas to the copper furnace), which is a manual process and may differ by several minutes depending on the exact size of each sample. Finally, air samples analyzed using this early trial displayed no bias nor loss in precision relative to air samples analyzed using the presented method.

The key difference between air and water samples is that air samples contain minimal water vapor (several percent of total gas, depending on the humidity at the time of collection) while water samples contain a small amount of residual water after draining (on the order of 1 mL) that evaporates throughout sample processing, providing a much larger flux of water vapor to the trap and allowing for the formation of ice. Naturally, ice is also formed in the presented version of the method when the trap is held at −95°C to −105°C, but critically, it is the temperature of ice in the trap that governs the adsorptivity of N_2, Ar, and Kr. In other words, despite the formation of ice in the water trap in both methods, we suspect that the much colder temperature of ice in the early trial led to substantial adsorptive loss of Kr and Ar (and likely minimal loss of N_2). The agreement of N_2/Ar in the presented version of the method with published solubility data, as well as other methodological studies that indicate no adsorptive loss of N_2, Ar, or Kr when using a glass trap at approximately −100°C [24, 34], provides confidence in our final presented version of the method.

4 | Determination of the Solubility Equilibrium N_2 Isotope Effect in Water

For application of dissolved $\delta^{15}N\text{-}N_2$ as a biogeochemical tracer in aquatic systems, it is essential to precisely know the $\delta^{15}N\text{-}N_2$ of water at solubility equilibrium with air, as any biogeochemical signals in water are quantified as a deviation from the solubility equilibrium. Pioneering work in the 1960s demonstrated that $^{29}N_2$ is slightly more soluble than $^{28}N_2$ in fresh water, exhibiting a solubility equilibrium fractionation that decreases with temperature [25]. These experiments were carried out with an analytical uncertainty of ~0.1‰. Subsequent work by Benson and Krause [27], which was unpublished but included in [40], and by Emerson et al. [26] further constrained the N_2 SEIE with improved precision (0.02‰–0.03‰). Experiments by Emerson et al. also showed that $\delta^{15}N\text{-}N_2$ was equal to within analytical precision in air-equilibrated 10°C freshwater and saltwater (salinity of 33 psu). Detecting biogeochemical signals in aquatic systems at the 0.01‰ level and below, however, requires resolution of the SEIE at the order-0.001‰ scale.

Here, we present an analysis of the results from the seven air–water equilibration experiments ($n = 35$ samples) summarized in Table 1 to determine the N_2 SEIE in water. Following standard isotope terminology, we define the fractionation factor, α_{sol}, as follows:

$$\alpha_{sol} = \frac{\left({}^{29}N_2/{}^{28}N_2\right)_{diss}}{\left({}^{29}N_2/{}^{28}N_2\right)_{gas}} \quad (5)$$

where the subscripts diss and gas refer to dissolved and gas phases, respectively, and such that α_{sol} is the reaction constant for the equilibrium reaction of isotopic substitution between dissolved N_2 and a free gas phase. Our measurements of $\delta^{15}N\text{-}N_2$ from air–water equilibration experiments therefore provide an estimate of ε_{sol} (where $\varepsilon = \alpha - 1$), because measured δ values are reported relative to the mean of atmospheric air measurements. Figure 6 shows a summary of ε_{sol} as a function of experiment temperature, alongside prior measurements from the aforementioned studies.

We find a coherent linear dependence of ε_{sol} on temperature based on our measurements, which closely follows the line of best fit given as follows ($R^2 = 0.91$):

$$\varepsilon_{sol}(‰) = 0.753 - 0.004T \quad (6)$$

In Data S1, we provide a table of ε_{sol} and its uncertainty (±1 SE) at 0.1°C intervals between 0°C and 25°C for application in aquatic systems. The uncertainty of the fitted line ranges from 0.001‰ to 0.002‰ over this range, which accomplishes a crucial step toward application in natural environments. The leading source of uncertainty in resolving a biogeochemical dissolved $\delta^{15}N\text{-}N_2$ signal is now the analytical uncertainty of a measurement (0.006‰), rather than the background solubility equilibrium isotopic composition of N_2 in water.

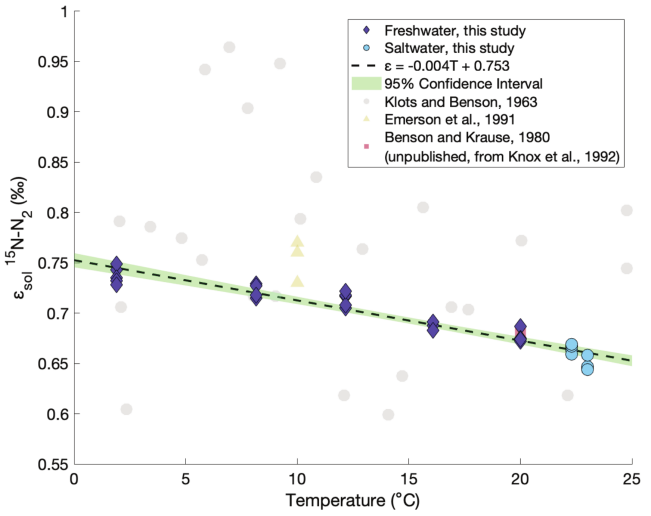

FIGURE 6 | Solubility equilibrium isotope effect of dissolved N_2 in water (ε_{sol} $^{15}N\text{-}N_2$) as a function of temperature for freshwater and UV-sterilized seawater samples. Shown here are prior measurements [25–27] along with our new determinations. Also included is a line of best fit and 95% confidence interval constrained by the 35 measurements in this study.

The N_2 SEIE is similar in sign and magnitude to SEIEs of other monatomic and diatomic gases (e.g., He, Ne, Ar, Kr, Xe, O_2, and H_2), which also exhibit a reduction in magnitude with increasing temperature [27–30, 41–44]. Surprisingly, we do not observe any significant difference between N_2 isotope SEIE values measured in salty water (~30 psu) and fresh water, unlike the small but well-constrained enhancement of SEIE with salinity measured and simulated for noble gas isotopes [27, 29, 30, 45]. As the small salinity effects for Ar, Kr, and Xe are known to increase quasi-linearly with increasing salinity, our findings suggest a negligible influence of salinity on the N_2 SEIE when extrapolated to the mean salinity of seawater (~35 psu) [30, 46]. This is a convenient result for the application of $\delta^{15}N\text{-}N_2$ in natural aquatic systems, as Equation (6) should hold equally well in freshwater and seawater environments and across salinity gradients.

To our knowledge, only Dang et al. [45] have explored the physical chemistry origin of the N_2 SEIE in water, implementing a classical molecular dynamics framework to simulate an ε_{sol} value of 0.93‰ in freshwater at 295 K, which is of the same sign and approximate magnitude as our results. Dang et al. decompose this effect into contributions from restricted translation (+0.92‰), rotation (+0.42‰), and vibration (−0.41‰) of an N_2 molecule occupying a solvation shell in water, finding that the latter two effects cancel, leaving translation as the primary contributing factor to the N_2 SEIE [45]. In this sense, it is unsurprising that the N_2 SEIE exhibits behavior similar to that of noble gases, which, being monatomic gases, do not exhibit rotational or vibrational motion. We suggest that future molecular dynamics experiments following the approach of Dang et al. [45] and Seltzer et al. [30] may shed light on the divergent behavior of noble gas and N_2 SEIEs in response to increasing salinity.

5 | Future Improvements and Applications to Natural Aquatic Systems

We have developed and evaluated a new method to measure high-precision isotopes of dissolved N_2 paired with measurements of $\delta(N_2/Ar)$, $\delta(^{40}Ar/^{36}Ar)$, and $\delta(Kr/N_2)$ in water. This method will allow for the characterization of biogeochemical and physical isotopic fractionation of N_2 in water at the order-0.001‰ scale, opening the door to new applications in aquatic systems. In particular, the combination of high-precision N_2 isotopes with Ar and Kr constraints will enable deconvolution of physical and biogeochemical anomalies from the background solubility equilibrium isotopic composition of N_2 in water, which we have now precisely redetermined (Figure 6).

This new technique holds promise in constraining the budget and cycling of fixed nitrogen in the ocean interior. Whereas the few existing prior studies have largely focused on oxygen minimum zones [7–9, 11, 12], where fixed nitrogen consumption is complete and excess (biogenic) N_2 is maximal, the magnitude and biogeochemical pathways of fixed N loss in partially oxygenated portions of the ocean remain underexplored yet are potentially important to the global budget of marine nitrogen [17, 18]. Although signals of denitrification are often large in coastal environments, these measurements can still be used in conjunction with other nitrogen-cycling measurements, such as nitrate and N_2O isotopes, to better understand the overall cycling and nitrogen budgets of these systems.

Our method also has the potential to aid in constraining the sources and pathways of denitrification in groundwater and lake environments, where N_2/Ar ratios have previously been used to quantify excess N_2 [47–51]. For example, the addition of Kr/Ar ratios will help quantitatively separate denitrification signals from excess air, both of which increase N_2/Ar in groundwater. This is because the injection of excess air (e.g., from entrainment of air bubbles during groundwater recharge and subsequent dissolution under hydrostatic pressure) leads to greater supersaturation of less soluble gases. Because Kr and Ar are inert and differ in solubility by a factor of two [33], they represent ideal tracers to constrain the solubility-dependent excess air effect and thereby correct N_2/Ar to better quantify denitrification signals. Similarly, the addition of N_2 isotopes may provide a powerful constraint on the origin of nitrate in groundwater, as excess N_2 is often observed in anoxic groundwaters in which the conversion of nitrate to N_2 is quantitative. In these cases, the inferred isotopic composition of N_2 in groundwater will be indicative of the N_2 composition of nitrate, which may aid in studies focused on nitrogen pollution of groundwater systems.

Finally, we identify several opportunities for further improvement of the analytical method. We note that the $\delta^{15}N\text{-}N_2$ reproducibility of air and water samples in our study was approximately equal to that of internal reference gas analyses (i.e., Can 2 vs. Can 1), indicating that the leading source of uncertainty is not the sampling, storage, or processing of gases but rather the analysis on the refurbished Thermo MAT 253 mass spectrometer in our laboratory. Applying our technique using a higher performance IRMS instrument with a dedicated collector array for simultaneous detection of $^{29}N_2$, $^{28}N_2$, ^{36}Ar, and ^{40}Ar would eliminate the need for magnetic peak jumping to measure the N_2/Ar ratio and allow for analysis of Ar isotope ratios at the same time as N_2 isotope ratios, thereby wasting less gas and enabling increased analytical precision. We also suggest that the addition of rare isotope spikes (^{21}Ne, ^{38}Ar, and ^{78}Kr) would allow for high-precision measurement of absolute Ar, Ne, and Kr abundances, which, along with high-precision N_2/Ar measurements, would facilitate robust measurements of the abundances of Ne, Ar, N_2, and Kr in a single sample. This addition could provide further information that could aid in resolving barometric pressure at the point of air–water equilibration, for example. Our development of a method for high-precision $\delta^{15}N\text{-}N_2$ and the refinement of the N_2 isotopic solubility function in water are perhaps just the first step toward many new applications of paired N_2-noble gas measurements in natural aquatic systems.

Author Contributions

Katelyn McPaul: conceptualization, data curation, formal analysis, investigation, writing – original draft, methodology, software, visualization, validation, writing – review and editing. **Scott D. Wankel:** funding acquisition, resources, supervision, writing – review and editing. **Alan M. Seltzer:** conceptualization, funding acquisition, writing – original draft, project administration, methodology, validation, data curation, supervision, resources, software, formal analysis, visualization, writing – review and editing.

Acknowledgments

We thank Josh Curtice, Dempsey Lott, Kevin Cahill, and Bill Jenkins for the technical assistance with the air–water equilibration systems and fabrication of the vacuum processing line, Rachel Stanley for the generous loaning of equipment, Bonnie Chang for the helpful theoretical discussions, and Israela Musan and Grace Brown for the support in sample collection. We are grateful to the US National Science Foundation (Award # OCE-2318938) and The Andrew W. Mellon Foundation Endowed Fund for Innovative Research for supporting this work. Open Access funding enabled and organized by MIT Hybrid 2025.

Data Availability Statement

All data in this study are available in tables in the manuscript and/or Data S1.

Peer Review

The peer review history for this article is available at https://www.webofscience.com/api/gateway/wos/peer-review/10.1002/rcm.10094.

References

1. D. M. Sigman, K. L. Casciotti, M. Andreani, C. Barford, M. Galanter, and J. K. Böhlke, "A Bacterial Method for the Nitrogen Isotopic Analysis of Nitrate in Seawater and Freshwater," *Analytical Chemistry* 73, no. 17 (2001): 4145–4153, https://doi.org/10.1021/ac010088e.

2. J. Granger, D. M. Sigman, M. M. Rohde, M. T. Maldonado, and P. D. Tortell, "N and O Isotope Effects During Nitrate Assimilation by Unicellular Prokaryotic and Eukaryotic Plankton Cultures," *Geochimica et Cosmochimica Acta* 74, no. 3 (2010): 1030–1040, https://doi.org/10.1016/j.gca.2009.10.044.

3. S. D. Wankel, C. Buchwald, W. Ziebis, C. B. Wenk, and M. F. Lehmann, "Nitrogen Cycling in the Deep Sedimentary Biosphere: Nitrate Isotopes in Porewaters Underlying the Oligotrophic North Atlantic," *Biogeosciences* 12, no. 24 (2015): 7483–7502, https://doi.org/10.5194/bg-12-7483-2015.

4. K. L. Casciotti, M. Forbes, J. Vedamati, B. D. Peters, T. S. Martin, and C. W. Mordy, "Nitrous Oxide Cycling in the Eastern Tropical South Pacific as Inferred From Isotopic and Isotopomeric Data," *Deep Sea Research Part II: Topical Studies in Oceanography.* 156 (2018): 155–167, https://doi.org/10.1016/j.dsr2.2018.07.014.

5. E. M. Baggs, "A Review of Stable Isotope Techniques for N_2O Source Partitioning in Soils: Recent Progress, Remaining Challenges and Future Considerations," *Rapid Communications in Mass Spectrometry* 22, no. 11 (2008): 1664–1672, https://doi.org/10.1002/rcm.3456.

6. B. B. Benson and P. D. M. Parker, "Nitrogen/Argon and Nitrogen Isotope Ratios in Aerobic Sea Water," *Deep Sea Research (1953)* 7, no. 4 (1961): 237–253, https://doi.org/10.1016/0146-6313(61)90042-9.

7. Fuchsman CA Murray JW Konovalov SK Concentration and Natural Stable Isotope Profiles of Nitrogen Species in the Black Sea *Marine Chemistry* 2008 111 1 90 105, https://doi.org/10.1016/j.marchem.2008.04.009.

8. C. C. Manning, R. C. Hamme, and A. Bourbonnais, "Impact of Deep-Water Renewal Events on Fixed Nitrogen Loss From Seasonally-Anoxic Saanich Inlet," *Marine Chemistry* 122, no. 1 (2010): 1–10, https://doi.org/10.1016/j.marchem.2010.08.002.

9. M. A. Altabet, E. Ryabenko, L. Stramma, et al., "An Eddy-Stimulated Hotspot for Fixed Nitrogen-Loss From the Peru Oxygen Minimum Zone," *Biogeosciences* 9, no. 12 (2012): 4897–4908, https://doi.org/10.5194/bg-9-4897-2012.

10. C. N. Charoenpong, L. A. Bristow, and M. A. Altabet, "A Continuous Flow Isotope Ratio Mass Spectrometry Method for High Precision Determination of Dissolved Gas Ratios and Isotopic Composition," *Limnology and Oceanography: Methods* 12, no. 5 (2014): 323–337, https://doi.org/10.4319/lom.2014.12.323.

11. A. Bourbonnais, M. A. Altabet, C. N. Charoenpong, et al., "N-Loss Isotope Effects in the Peru Oxygen Minimum Zone Studied Using a Mesoscale Eddy as a Natural Tracer Experiment," *Global Biogeochemical Cycles* 29, no. 6 (2015): 793–811, https://doi.org/10.1002/2014GB005001.

12. H. Hu, A. Bourbonnais, J. Larkum, H. W. Bange, and M. A. Altabet, "Nitrogen Cycling in Shallow Low-Oxygen Coastal Waters of Peru From Nitrite and Nitrate Nitrogen and Oxygen Isotopes," *Biogeosciences* 13, no. 5 (2016): 1453–1468, https://doi.org/10.5194/bg-13-1453-2016.

13. P. H. Barry and M. W. Broadley, "Nitrogen and Noble Gases Reveal a Complex History of Metasomatism in the Siberian Lithospheric Mantle," *Earth and Planetary Science Letters* 556 (2021): 116707, https://doi.org/10.1016/j.epsl.2020.116707.

14. J. P. Severinghaus, T. Sowers, E. J. Brook, R. B. Alley, and M. L. Bender, "Timing of Abrupt Climate Change at the End of the Younger Dryas Interval From Thermally Fractionated Gases in Polar Ice," *Nature* 391, no. 6663 (1998): 141–146, https://doi.org/10.1038/34346.

15. T. Sowers, M. Bender, and D. Raynaud, "Elemental and Isotopic Composition of Occluded O_2 and N_2 in Polar Ice," *Journal of Geophysical Research: Atmospheres* 94, no. D4 (1989): 5137–5150, https://doi.org/10.1029/JD094iD04p05137.

16. R. C. Hamme and S. R. Emerson, "The Solubility of Neon, Nitrogen and Argon in Distilled Water and Seawater," *Deep Sea Research Part I: Oceanographic Research Papers.* 51, no. 11 (2004): 1517–1528, https://doi.org/10.1016/j.dsr.2004.06.009.

17. D. Bianchi, T. S. Weber, R. Kiko, and C. Deutsch, "Global Niche of Marine Anaerobic Metabolisms Expanded by Particle Microenvironments," *Nature Geoscience* 11, no. 4 (2018): 263–268, https://doi.org/10.1038/s41561-018-0081-0.

18. R. C. Hamme and S. R. Emerson, "Deep-Sea Nutrient Loss Inferred From the Marine Dissolved N_2/Ar Ratio," *Geophysical Research Letters* 40, no. 6 (2013): 1149–1153, https://doi.org/10.1002/grl.50275.

19. A. M. Seltzer, D. P. Nicholson, W. M. Smethie, et al., "Dissolved Gases in the Deep North Atlantic Track Ocean Ventilation Processes," *National Academy of Sciences of the United States of America* 120, no. 11 (2023): e2217946120, https://doi.org/10.1073/pnas.2217946120.

20. A. H. Devol, A. G. Uhlenhopp, S. W. A. Naqvi, et al., "Denitrification Rates and Excess Nitrogen Gas Concentrations in the Arabian Sea Oxygen Deficient Zone," *Deep Sea Research Part I: Oceanographic Research Papers.* 53, no. 9 (2006): 1533–1547, https://doi.org/10.1016/j.dsr.2006.07.005.

21. B. X. Chang, A. H. Devol, and S. R. Emerson, "Denitrification and the Nitrogen Gas Excess in the Eastern Tropical South Pacific Oxygen Deficient Zone," *Deep Sea Research Part I: Oceanographic Research Papers.* 57, no. 9 (2010): 1092–1101, https://doi.org/10.1016/j.dsr.2010.05.009.

22. B. X. Chang, A. Jayakumar, B. Widner, et al., "Low Rates of Dinitrogen Fixation in the Eastern Tropical South Pacific," *Limnology and Oceanography* 64, no. 5 (2019): 1913–1923, https://doi.org/10.1002/lno.11159.

23. C. A. Fuchsman, A. H. Devol, K. L. Casciotti, C. Buchwald, B. X. Chang, and R. E. A. Horak, "An N Isotopic Mass Balance of the Eastern Tropical North Pacific Oxygen Deficient Zone," *Deep Sea Research Part II: Topical Studies in Oceanography.* 156 (2018): 137–147, https://doi.org/10.1016/j.dsr2.2017.12.013.

24. A. M. Seltzer and D. V. Bekaert, "A Unified Method for Measuring Noble Gas Isotope Ratios in Air, Water, and Volcanic Gases via Dynamic Mass Spectrometry," *International Journal of Mass Spectrometry* 478 (2022): 116873, https://doi.org/10.1016/j.ijms.2022.116873.

25. C. E. Klots and B. B. Benson, "Isotope Effect in the Solution of Oxygen and Nitrogen in Distilled Water," *Journal of Chemical Physics* 38, no. 1 (1963): 890–892.

26. S. Emerson, P. Quay, C. Stump, D. Wilbur, and M. Knox, "O_2, Ar, N_2, and 222Rn in Surface Waters of the Subarctic Ocean: Net Biological O_2 Production," *Global Biogeochemical Cycles* 5, no. 1 (1991): 49–69, https://doi.org/10.1029/90GB02656.

27. Table 1, Benson, and Krause, unpublished data (1980), in M. Knox, P. D. Quay, and D. Wilbur, "Kinetic Isotopic Fractionation During Air–Water Gas Transfer of O_2, N_2, CH_4, and H_2," *Journal of Geophysical Research, Oceans* 97, no. C12 (1992): 20335–20343, https://doi.org/10.1029/92JC00949.

28. K. E. Tempest and S. Emerson, "Kinetic Isotopic Fractionation of Argon and Neon During Air–Water Gas Transfer," *Marine Chemistry* 153 (2013): 39–47, https://doi.org/10.1016/j.marchem.2013.04.002.

29. A. M. Seltzer, J. Ng, and J. P. Severinghaus, "Precise Determination of Ar, Kr and Xe Isotopic Fractionation due to Diffusion and Dissolution in Fresh Water," *Earth and Planetary Science Letters* 514 (2019): 156–165, https://doi.org/10.1016/j.epsl.2019.03.008.

30. A. M. Seltzer, S. A. Shackleton, and I. C. Bourg, "Solubility Equilibrium Isotope Effects of Noble Gases in Water: Theory and Observations," *Journal of Physical Chemistry. B* 127, no. 45 (2023): 9802–9812, https://doi.org/10.1021/acs.jpcb.3c05651.

31. S. Emerson, C. Stump, D. Wilbur, and P. Quay, "Accurate Measurement of O_2, N_2, and Ar Gases in Water and the Solubility of N_2," *Marine Chemistry* 64, no. 4 (1999): 337–347, https://doi.org/10.1016/S0304-4203(98)00090-5.

32. J. Ng, R. Tyne, A. Seltzer, C. Noyes, J. McIntosh, and J. Severinghaus, "A New Large-Volume Equilibration Method for High-Precision Measurements of Dissolved Noble Gas Stable Isotopes," *Rapid Communications in Mass Spectrometry* 37, no. 7 (2023): e9471, https://doi.org/10.1002/rcm.9471.

33. W. J. Jenkins, D. E. Lott, and K. L. Cahill, "A Determination of Atmospheric Helium, Neon, Argon, Krypton, and Xenon Solubility Concentrations in Water and Seawater," *Marine Chemistry* 211 (2019): 94–107, https://doi.org/10.1016/j.marchem.2019.03.007.

34. J. P. Severinghaus, A. Grachev, B. Luz, and N. Caillon, "A Method for Precise Measurement of Argon 40/36 and Krypton/Argon Ratios in Trapped Air in Polar Ice With Applications to Past Firn Thickness and Abrupt Climate Change in Greenland and at Siple Dome, Antarctica," *Geochimica et Cosmochimica Acta* 67, no. 3 (2003): 325–343, https://doi.org/10.1016/S0016-7037(02)00965-1.

35. "Series 275 Digital Readout Convectron Vacuum Gauge Instruction Manual," Published online October 1999. Accessed January 17, 2025, https://www.idealvac.com/files/brochures/GP275_DigitalManual.pdf.

36. T. A. Sowers, M. L. Bender, D. Raynaud, and C. Lorius, "Elemental and Isotopic Composition of O_2 and N_2 Gases in Ice Cores," *Annals of Glaciology* 10 (1988): 218, https://doi.org/10.3189/S0260305500004651.

37. P. Sturm, M. Leuenberger, C. Sirignano, et al., "Permeation of Atmospheric Gases Through Polymer O-Rings Used in Flasks for Air Sampling," *Journal of Geophysical Research – Atmospheres* 109, no. D4 (2004): 1–9, https://doi.org/10.1029/2003JD004073.

38. R. H. R. Stanley and E. M. Howard, "Quantifying Photosynthetic Rates of Microphytobenthos Using the Triple Isotope Composition of Dissolved Oxygen," *Limnology and Oceanography: Methods* 11, no. 7 (2013): 360–373, https://doi.org/10.4319/lom.2013.11.360.

39. E. Leon-Palmero, R. Morales-Baquero, B. Thamdrup, C. Löscher, and I. Reche, "Sunlight Drives the Abiotic Formation of Nitrous Oxide in Fresh and Marine Waters," *Science* 387, no. 6739 (2025): 1198–1203, https://doi.org/10.1126/science.adq0302.

40. M. Knox, P. D. Quay, and D. Wilbur, "Kinetic Isotopic Fractionation During Air–Water Gas Transfer of O_2, N_2, CH_4, and H_2," *Journal of Geophysical Research, Oceans* 97, no. C12 (1992): 20335–20343, https://doi.org/10.1029/92JC00949.

41. B. Li, L. Y. Yeung, H. Hu, and J. L. Ash, "Kinetic and Equilibrium Fractionation of O_2 Isotopologues During Air–Water Gas Transfer and Implications for Tracing Oxygen Cycling in the Ocean," *Marine Chemistry* 210 (2019): 61–71, https://doi.org/10.1016/j.marchem.2019.02.006.

42. B. Benson, B and D. Krause, Jr., "The Concentration and Isotopic Fractionation of Oxygen Dissolved in Freshwater and Seawater in Equilibrium With the Atmosphere," *Limnology and Oceanography* 29, no. 3 (1984): 620–632, https://doi.org/10.4319/lo.1984.29.3.0620.

43. G. Jancsó, "Interpretation of Isotope Effects on the Solubility of Gases," *Nukleonika* 47, no. Suppl.1 (2002): 53–57.

44. J. Muccitelli and W. Y. Wen, "Solubilities of Hydrogen and Deuterium Gases in Water and Their Isotope Fractionation Factor," *Journal of Solution Chemistry* 7, no. 4 (1978): 257–267, https://doi.org/10.1007/BF00644273.

45. L. X. Dang, P. Bopp, and M. Wolfsberg, "Evaluation of Isotope Effectson Henry's Law Constants by a Molecular Dynamics Technique," *Zeitschrift für Naturforschung* 44, no. 5 (1989): 485–491, https://doi.org/10.1515/zna-1989-0519.

46. R. C. Hamme and J. P. Severinghaus, "Trace Gas Disequilibria During Deep-Water Formation," *Deep Sea Research Part I: Oceanographic Research Papers.* 54, no. 6 (2007): 939–950, https://doi.org/10.1016/j.dsr.2007.03.008.

47. J. C. Vogel, A. S. Talma, and T. H. E. Heaton, "Gaseous Nitrogen as Evidence for Denitrification in Groundwater," *Journal of Hydrology* 50 (1981): 191–200, https://doi.org/10.1016/0022-1694(81)90069-X.

48. G. Blicher-Mathiesen, G. W. McCarty, and L. P. Nielsen, "Denitrification and Degassing in Groundwater Estimated From Dissolved Dinitrogen and Argon," *Journal of Hydrology* 208, no. 1 (1998): 16–24, https://doi.org/10.1016/S0022-1694(98)00142-5.

49. L. J. Puckett, T. K. Cowdery, P. B. McMahon, L. H. Tornes, and J. D. Stoner, "Using Chemical, Hydrologic, and Age Dating Analysis to Delineate Redox Processes and Flow Paths in the Riparian Zone of a Glacial Outwash Aquifer-Stream System," *Water Resources Research* 38, no. 8 (2002): 9–9-20, https://doi.org/10.1029/2001WR000396.

50. J. M. Taylor, I. M. Andersen, A. K. Hoke, P. T. Kelly, and J. T. Scott, "In-Situ N2:Ar Ratios Describe the Balance Between Nitrogen Fixation and Denitrification in Shallow Eutrophic Experimental Lakes," *Biogeochemistry* 166, no. 3 (2023): 283–301, https://doi.org/10.1007/s10533-023-01063-6.

51. M. A. Coble, K. M. Rogers, J. Curtis, et al., "New Method for Measuring Dissolved Ne, Ar, and N_2 in Water Using a Plasma Emission Detector: Application for Quantifying Denitrification in Groundwater," *ACS ES&T Water* 4, no. 9 (2024): 3851–3862, https://doi.org/10.1021/acsestwater.4c00170.

Supporting Information

Additional supporting information can be found online in the Supporting Information section.